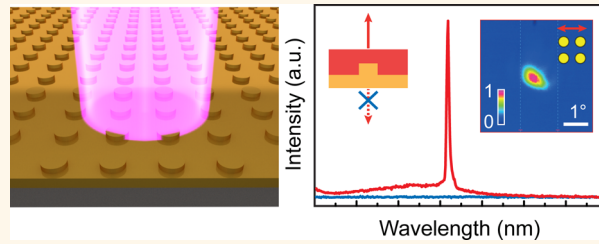


Unidirectional Lasing from Template-Stripped Two-Dimensional Plasmonic Crystals

Ankun Yang,[†] Zhongyang Li,[‡] Michael P. Knudson,[†] Alexander J. Hryn,[†] Weijia Wang,[§] Koray Aydin,[‡] and Teri W. Odom^{*,†,§,||}

[†]Department of Materials Science and Engineering, Northwestern University, Evanston, Illinois 60208, United States, [‡]Department of Electrical Engineering and Computer Science, Northwestern University, Evanston, Illinois 60208, United States, [§]Graduate Program in Applied Physics, Northwestern University, Evanston, Illinois 60208, United States, and ^{||}Department of Chemistry, Northwestern University, Evanston, Illinois 60208, United States

ABSTRACT Plasmon lasers support cavity structures with sizes below that of the diffraction limit. However, most plasmon-based lasers show bidirectional lasing emission or emission with limited far-field directionality and large radiative losses. Here, we report unidirectional lasing from ultrasMOOTH, template-stripped two-dimensional (2D) plasmonic crystals. Optically pumped 2D plasmonic crystals (Au or Ag) surrounded by dye molecules exhibited lasing in a single emission direction and their lasing wavelength could be tuned by modulating the dielectric environment. We found that 2D plasmonic crystals were an ideal architecture to screen how nanocavity unit-cell structure, metal material, and gain media affected the lasing response. We discovered that template-stripped strong plasmonic materials with cylindrical posts were an optimal cavity design for a unidirectional laser operating at room temperature.



KEYWORDS: plasmon nanolaser · spaser · plasmonic crystals · unidirectional emission · template stripping · wavelength tunability

Surface plasmons are coherent oscillations of free electrons at a metal-dielectric interface that can trap free-space light as surface plasmon polaritons (SPPs).¹ SPPs with confined and enhanced electromagnetic (EM) fields are promising for compact photonic circuits because of their strong optical field localization.² The primary challenge in exploiting SPPs in devices, however, is their short lifetimes from their large energy dissipation in metals.³ One approach to increase lifetime is to compensate the losses (*i.e.*, scattering and absorption) with gain materials such as organic dyes and inorganic semiconductors.⁴ Another strategy to mitigate loss is clever design of the structure and arrangement of the metallic nanostructures.^{5–7} For example, plasmonic nanoparticles (NPs) arranged into one-dimensional (1D) and two-dimensional (2D) arrays can suppress radiative losses of isolated NPs and support lattice plasmon resonances that exhibit much higher quality factors ($Q > 200$) compared to a single NP ($Q < 20$).^{5,8–11}

A plasmonic nanolaser, or spaser (surface plasmon amplification by stimulated emission of radiation), is a device based on plasmonic cavities and gain media that can compensate loss and achieve amplification of nanolocalized EM fields.^{12,13} Plasmonic nanolasers can overcome the diffraction limit and act as coherent light sources with nanoscale dimensions for miniaturized photonic devices.² Several nanocavity architectures have been reported for spasers.^{14–16} In the metal film-dielectric spacer-semiconductor nanowire configuration,^{14,17} the metal film substrate both supports an SPP mode that behaves as the lasing cavity and confines the emission into the space above the surface. The light tends to scatter most strongly from the microscale Fabry-Pérot cavity at nanowire end-facets with little or no directionality. An advantage of the metal film in this spaser architecture is the possibility of electrical pumping as well as heat sinking.¹⁸ Moreover, crystalline plasmonic films can reduce losses due to scattering, but a drawback is that the preparation of high-quality metal films involves multistep processes

* Address correspondence to todom@northwestern.edu.

Received for review August 28, 2015 and accepted October 11, 2015.

Published online October 11, 2015
10.1021/acsnano.5b05419

© 2015 American Chemical Society

such as low-temperature deposition followed by room-temperature annealing.^{17,19}

Another architecture for nanolasers is arrays of plasmonic cavities, where the unit cell building blocks are NPs or nanoholes.^{8,16,20–22} Although predicted to exhibit directional far-field emission normal to the surface,⁶ such plasmonic crystals show bidirectional lasing, where half the emitted light is not collected and is essentially wasted.^{16,20–22} Nevertheless, because metal NP arrays can support lattice plasmons that are sensitive to dielectric environment, real-time and tunable lasing emission is possible for a static NP array structure and substrate.⁸ One challenge for using lattice plasmons as feedback is that the lasing quality is highest when the dielectric environment above and below the NPs is index-matched;⁵ thus, for a fixed NP array and substrate, there are constraints on the potential gain media accessible for a nanolasering.

Here, we show that unidirectional, tunable lasing can be obtained from template-stripped 2D plasmonic crystals. 2D plasmonic crystals combine the advantages of a metal film and NP arrays and show lasing in a single emission direction. Template stripping from a single-crystalline silicon master provides a scalable approach to produce uniform plasmonic crystal substrates with ultrasMOOTH metal surfaces. We established the design principles for an optimized unidirectional lasing device by examining different plasmonic materials, unit cell shapes, and gain materials. We found that lasing was strongest in plasmonic crystals (Au, Ag) with cylindrical posts and that emission could be tuned by incorporating different gain media on the same substrate.

RESULTS AND DISCUSSION

Figure 1a depicts the fabrication procedure to prepare 2D plasmonic crystals using template stripping, where the scheme indicates plasmonic crystals consisting of a metal film with protruding metal posts. First, we defined aluminum hole arrays (spacing $a_0 = 600$ nm, diameter $d = 200$ nm) on Si (100) wafers by (1) patterning photoresist post arrays via phase-shifting photolithography,²³ (2) depositing a thin layer of Al (7 nm); and (3) lifting off the resist. The natural oxidation of Al resulted in a layer of aluminum oxide ($\text{Al}_x\text{O}_y < 5$ nm)²⁴ that could function as a highly selective etching mask for deep reactive ion etching (DRIE).²⁵ After DRIE through the Al_xO_y hole array to a depth h and removal of the alumina mask, we obtained a Si template with 600 nm periodic holes ($d = 200$ nm) that could be reused multiple times to template-strip plasmonic crystals with identical features. Finally, we deposited metal into the template using a thermal evaporator and then stripped the nanopatterned film using polyurethane (PU, NOA 61, Norland Products) (Figure 1b). Thick Au films were deposited (~ 150 nm)

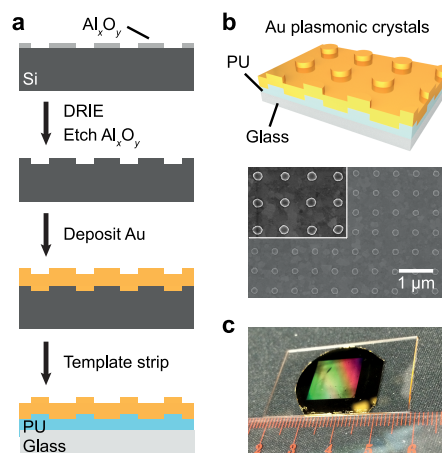


Figure 1. UltrasMOOTH 2D plasmonic crystals based on template stripping. (a) Scheme for fabrication. (b) Cartoon and SEM (inset: $2.2 \times 1.6 \mu\text{m}^2$) of Au plasmonic crystals with cylindrical posts ($a_0 = 600$ nm, $d = 200$ nm, $h = 35$ nm). (c) Photograph of 2D Au plasmonic crystals.

to ensure that the thinnest part of the structure was ca. 100 nm, much larger than the skin-depth of Au (<25 nm) at visible to near-IR frequencies²⁶ and to prevent field penetration and mode coupling between the top and bottom surfaces.²⁷ Scanning electron microscopy (SEM) and atomic force microscopy (AFM) images demonstrated that the surfaces of both the film and the protruding posts had subnanometer roughness (Figure S1). Our fabrication procedure based on template stripping can produce samples with areas larger than 1 cm^2 (Figure 1c).

SPP modes supported by 2D Au plasmonic crystals were characterized by an inverted optical microscope equipped with a spectrometer (Methods). Normal-incidence reflectance was measured in dimethyl sulfoxide (DMSO) as the dielectric environment (Figure 2a), a common solvent for dye molecules.⁸ This sample with $h = 35$ nm supported a SPP resonance at $\lambda_{\text{SPP}} = 882$ nm, which was in good agreement with finite-difference time-domain (FDTD) calculations (Methods). At the resonant wavelength, the near-field profiles showed a characteristic SPP wave pattern and strong field localization around the protruding posts (Figure 2a, inset). In general, SPP modes can be described by

$$\text{Re} \left[\frac{\omega}{c} \sqrt{\frac{\varepsilon_m \varepsilon_d}{\varepsilon_m + \varepsilon_d}} \right] = |k_0 \sin \theta + i\mathbf{G}_x + j\mathbf{G}_y|$$

where ω , c , and k_0 are the angular frequency, speed, and momentum of free-space light. ε_m and ε_d are the relative permittivity of the metal and dielectric, where $|\varepsilon_m| \gg |\varepsilon_d|$, and $\varepsilon_d = n^2$ for nonabsorbing materials (n : refractive index). The integer index pairs (i, j) denote specific SPP modes, and θ is the excitation angle. \mathbf{G}_x and \mathbf{G}_y are reciprocal vectors of the 2D grating, where $|\mathbf{G}_x| = |\mathbf{G}_y| = 2\pi/a_0$, and a_0 is periodicity. In the case of first-order normal-incidence modes, where $(i, j) = (\pm 1, 0)$

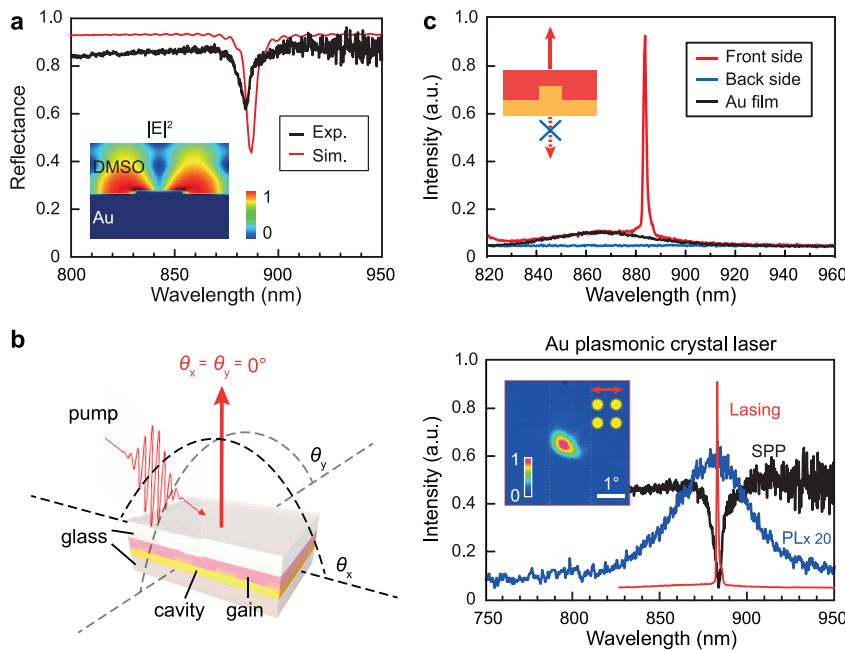


Figure 2. Unidirectional lasing from 2D Au plasmonic crystals. (a) SPP mode of 2D Au plasmonic crystals. Inset shows the near-field profile on resonance. (b) Left, scheme for the lasing measurement; right, photoluminescence (PL) of the IR-140 dye (blue), SPP resonance (black) and lasing spectrum (red) of a Au plasmonic crystal laser (pump power 20 mW). Inset shows the far-field profile of the lasing beam. (c) The lasing signal was captured only on the front side (red curve) coming from the protruding posts side. IR-140 dye molecules on flat template-stripped Au film only showed a PL spectrum (black curve).

or $(0, \pm 1)$, and $\theta = 0^\circ$, the SPP wavelength can be simplified to $\lambda_{\text{SPP}} = a_0[(\epsilon_m \epsilon_d)/(\epsilon_m + \epsilon_d)]^{1/2} = 889 \text{ nm}$, in agreement with FDTD simulations (888 nm). The slight mismatch of the experimental resonance ($\lambda_{\text{SPP}} = 882 \text{ nm}$) and these calculations can be attributed to differences in the fabricated unit-cell structure (size, shape) compared to the perfect structure used in simulations.

We constructed lasing devices by coating the Au plasmonic crystals with IR-140 dye molecules dissolved in DMSO (concentration: 5 mM) (Figure 2b). The samples were pumped with an 800 nm fs-pulsed laser (laser beam size $\sim 0.2 \text{ cm}^2$), and the emission was collected normal to the sample surface (Methods). Au plasmonic crystals exhibited lasing at $\lambda_{\text{lasing}} = 882 \text{ nm}$ with a full-width-at-half-maximum (fwhm) of 1.1 nm. The lasing wavelength was in good agreement with the SPP resonance of the same substrate characterized by reflectance measurements ($\lambda_{\text{SPP}} = 882 \text{ nm}$). In addition, the far-field emission had a divergence angle $< 1^\circ$ (Figure 2b, inset) and was more tightly focused compared to beam-profile measurements of lasing from plasmonic NP arrays.^{8,16} Because the Au substrate was optically thick and its smooth surface behaved like a mirror, lasing emission was on the same side as the pump source and gain media (Figure 2c). Measurements from the back side of the sample showed no signature of lasing or even photoluminescence. As a control, a flat gold film was prepared with dye on the superstrate, but no lasing emission was observed (Figure 2c).

To study the influence of the posts on the lasing performance, we fabricated three other types of samples: (1) Au posts (NPs) deposited through nanohole arrays²⁸ on template-stripped Au films; (2) template-stripped Au pyramid arrays; and (3) nonplasmonic Ti posts (NPs) deposited through nanohole arrays on template-stripped Au films. We selected these samples to compare the effects of different structures (roughness and shape) and materials (plasmonic and nonplasmonic) (Figure S2) on the plasmon-exciton energy transfer properties. Note: since all the samples share a common template-stripped Au film substrate, for brevity and clarity, we will denote them as (1) deposited Au posts, (2) stripped Au pyramids, and (3) deposited Ti posts. For example, template-stripped plasmonic crystals as in Figure 1 would be referred to as stripped Au posts.

Reflectance measurements showed that stripped Au posts exhibited both narrower and stronger resonances compared to deposited Au posts (fwhm = 11 and 13 nm, respectively) (Figure S2), consistent with FDTD simulations (Methods). The near-field profiles showed maximum field enhancement around the protruding Au posts ($|E|^2/|E_0|^2 = 10^3$) for both structures. With cavity loss ($\omega n/cQ$,²⁹ where n is refractive index and $Q = \omega/\Delta\omega$ is the quality factor) proportional to the fwhm of the resonance, stripped Au posts were less lossy compared to deposited Au posts with rough surfaces. In terms of shape effects, although stripped Au pyramids had stronger resonances compared to

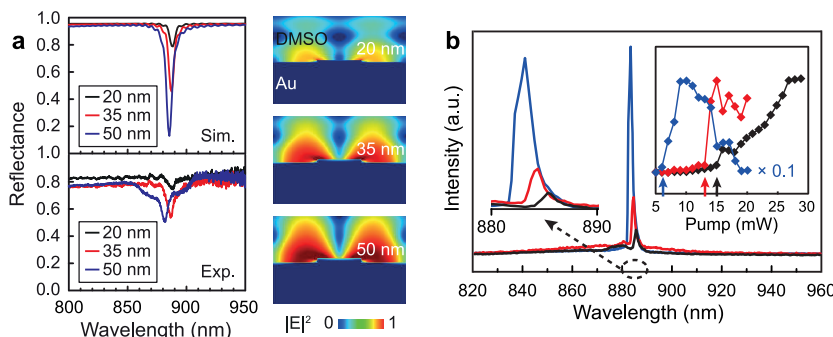


Figure 3. Au plasmonic crystals with different protruding post heights show varying lasing characteristics. (a) Simulated and measured reflectance of Au plasmonic crystals with post height $h = 20, 35$, and 50 nm ($a_0 = 600\text{ nm}$, $d = 200\text{ nm}$) in DMSO environment. All intensities were normalized to the same log scale. (b) SPP lasing wavelengths blue-shifted as a function of the post height; the input–output curves exhibited clear thresholds that decreased with increasing post height (inset, the arrows denote the threshold value). For the lasing spectra, the pump power was 15 mW for Au plasmonic crystals with 35 and 50 nm protruding posts and 20 mW for Au plasmonic crystals with 20 nm protruding posts.

stripped Au posts, they had much wider line widths ($\text{fwhm} = 34\text{ nm}$), reduced confinement of local fields, and lower EM field enhancements ($|E|^2/|E_0|^2 = 10^2$). Nonplasmonic substrates of deposited Ti posts had the weakest resonance and local field enhancement ($|E|^2/|E_0|^2 = 10$) compared to either stripped Au posts or deposited Au posts.

When integrated into a lasing device with the same gain materials, deposited Au posts showed lasing emission with broader line widths ($\lambda_{\text{lasing}} = 887\text{ nm}$, $\text{fwhm} = 3.5\text{ nm}$, Figure S3) compared to stripped Au posts. Moreover, the threshold level for deposited Au posts was slightly higher (8 mW , Figure S4) compared to the stripped samples ($\sim 5\text{ mW}$) because of scattering losses from the rough edges (Figure S4, inset). Interestingly, stripped Au pyramids only supported amplified spontaneous emission (ASE, Figure S3); this distinct behavior compared to the other two Au plasmonic crystals highlights the critical role of the local field enhancement. The protruding posts acted as collectors and concentrators of EM fields, and cylindrical shapes were more efficient for building-up charges compared to the pyramidal shapes with sloped sidewalls (Figure S5). Finally, deposited Ti posts with the least field enhancement showed ASE with weak intensities (Figure S3). Therefore, the desirable structural shape for protruding posts is cylindrical, and as expected, strongly plasmonic materials are needed to produce strong local field enhancements.

To study the effects of post height on the quality of the SPP mode and lasing signal, we selected template-stripped Au plasmonic crystals with cylindrical posts (stripped Au posts) and varied the height ($h = 20, 35$, and 50 nm). Figure 3a shows the simulated and measured reflectance of Au plasmonic crystals at normal incidence in a DMSO environment. As h was increased from 20 to 50 nm , the SPP resonance intensity increased from $\sim 5\%$ to $\sim 20\%$ in DMSO and from $\sim 10\%$ to $\sim 40\%$ in air (Figure S6). The spectral

location of the SPP resonances blue-shifted as the protrusion height increased, and the intensity of the local field enhancement also increased with post height. The majority of the EM fields extended into the DMSO dielectric layer.

We tested how changes in far-field and near-field linear optical properties of template-stripped Au plasmonic crystals affected the lasing response. At similar pump powers, Au plasmonic crystals with 50 nm protruding posts exhibited stronger emission intensities compared to Au plasmonic crystals with 35 and 20 nm posts (Figure 3b). The pump power vs output intensity curves exhibited a characteristic threshold behavior with a dramatic change in slope; the threshold values for Au plasmonic crystals with $20, 35$, and 50 nm protruding posts decreased from $15, 13$, to 6 mW (Figure 3b, inset). (We needed to pump with higher intensities to reach threshold for Au plasmonic crystals with 20 nm posts.) The protruding posts concentrated EM fields mostly on the top edges (Figure 3a). With increased post height, the local fields were more enhanced and lifted farther away from the metal surface; we hypothesize that both factors contributed to the reduced lasing thresholds. For 50 nm protruding post Au plasmonic crystals, at pump powers far above threshold, the output intensity dropped. This decrease can be attributed to the excitation of other competing loss channels^{8,16} as well as possible reduced dye integrity from local heating of the metal posts. Interestingly, the lasing emission also showed a minor and gradual blue shift ($\lambda_{\text{lasing}} = 885, 884$, and 883 nm , respectively) with increasing post height, consistent with the trends of the SPP resonance shift (Figure 3a). These different lasing characteristics for Au plasmonic crystals with different post heights again confirm the important role of the SPP mode and the unit cell size and shape for unidirectional lasing.

During the process of energy transfer from dye molecules to plasmons, molecules in an excited state

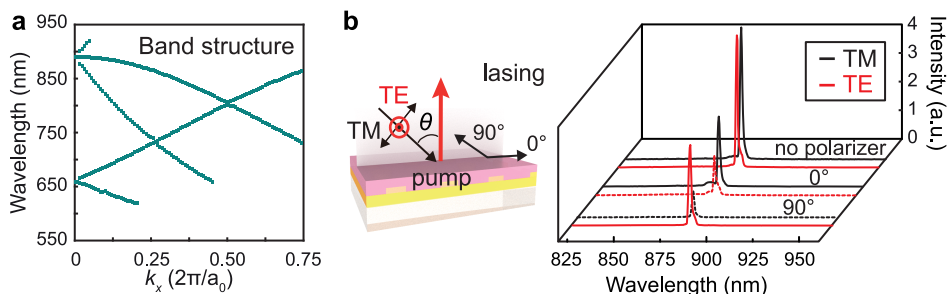


Figure 4. SPP wave serving as the lasing cavity. (a) Calculated band structure with dipole source excitation. (b) Lasing output at different angles under TM (transverse magnetic) and TE (transverse electric) pump.

can be modeled as dipole emitters;^{30,31} therefore, we simulated randomly distributed dipole sources to excite the Au plasmonic crystals to obtain the resulting band structure accessible to the excited dye molecules (Figure 4a). The band structure matched well with both the experimental data and plane-wave simulations (Figure S7), indicating that SPP modes were the dominate modes into which the dye molecules transferred their energy. We characterized the polarization of the lasing emission under both transverse magnetic (TM) and transverse electric (TE) pump conditions (Figure 4b) and found that the output lasing emission was polarized preferentially along the pump beam polarization. Pumped with TM polarization, the output beam of the lasing device had polarization along 0°, which was the same polarization direction as the TM SPP mode (Figure S8). Similarly, pumped by TE polarization, the output beam had a polarization along 90°, which was the same polarization as the TE SPP mode. The pump laser polarized in either TM and TE will preferentially excite dye molecules whose transition dipole moments are oriented parallel to the polarization; these contributions will dominate the lasing signal. Dye molecules oriented at angles θ relative to the pump polarization, however, can also be excited to produce low (probability $\propto \cos^2 \theta$) levels of emission in the perpendicular polarization direction. The preference of the output polarization can be clearly observed when a linear polarizer filter placed between the spectrometer and the lasing device is rotated (Movie S1).

On the basis of the simplicity of the SPP lasing cavity platform, we explored the effects of different materials for both the cavity and gain media. As another commonly used plasmonic material, Ag has much smaller imaginary part of the dielectric function compared to Au and is thus less lossy at visible and near-infrared wavelengths.¹ We fabricated Ag plasmonic crystals following the procedure described in Figure 1 and kept all the structural parameters the same (film thickness: $t = 150$ nm, $h = 35$ nm, $d = 200$ nm) (Figure 5a). Figure 5b shows a Ag plasmonic crystal device ($h = 35$ nm) lasing at its SPP resonance wavelength. Compared to Au plasmonic crystals with the same post height, the lasing emission ($\lambda_{\text{lasing}} = 881$ nm) was at

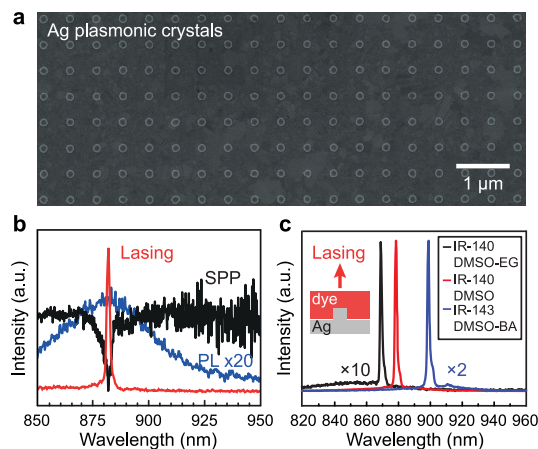


Figure 5. Ag plasmonic crystal lasers. (a) SEM images of Ag plasmonic crystals. (b) Lasing observed at the Ag SPP resonant wavelength (dye concentration, 5 mM) and (c) tunable lasing emission with different dye in different solvents (dye concentration, 2.5 mM; nominal refractive indices; 1.44, 1.48, 1.52).

shorter wavelengths. Moreover, at the same pump powers (20 mW), the emission intensity was ~1.5 times that of Au plasmonic crystals. Similar to Au substrates, Ag plasmonic crystals exhibited a decreased lasing threshold as the height of the posts increased. The polarization of the output emission from Ag plasmonic crystal lasers was also preferentially along the pump beam polarization (Figure S9).

Our plasmonic crystals can be used to screen and test different gain media. With the same Ag plasmonic crystals, we prepared IR-140 in a mixture of DMSO and ethylene glycol (EG) as gain medium and obtained lasing at shorter wavelength ($\lambda_{\text{lasing}} = 870$ nm) in contrast to the lasing from IR-140-DMSO at $\lambda_{\text{lasing}} = 879$ nm. Using the different dye molecule IR-143 in a mixture of DMSO and benzyl alcohol (BA), we achieved lasing at even longer wavelengths ($\lambda_{\text{lasing}} = 899$ nm) (Figure 5c). At the same pump power, lasing from IR-140-DMSO had the strongest emission since DMSO can better solubilize IR-140 and IR-143 compared to EG and BA. The tunability of the lasing emission originated from the change of the dielectric environment and the corresponding shift in SPP resonant wavelength.

CONCLUSION

In summary, we designed and realized a plasmon nanolaser with unidirectional emission. We developed a simple and scalable fabrication technique based on template stripping and produced uniform 2D plasmonic crystals with ultrasmooth surfaces, where protruding cylindrical posts with heights that lifted EM enhancement farthest away from the metal surface exhibited the strongest lasing performance. We conclude, based on structure and material screening, that SPPs can provide feedback for nanolasing, and the

concentration of local EM fields by cylindrical posts made from plasmonic materials will result in the lowest lasing thresholds and highest lasing intensity. In these 2D plasmonic crystal lasers, lasing wavelengths were tuned by changing different gain media (dye and/or solvent combinations). Compatible with large-scale nanomanufacturing techniques, 2D plasmonic crystals provide a platform to screen materials combinations for new classes of plasmon nanolasers, including those based on quantum emitters and inorganic semiconducting materials.

METHODS

Fabrication of Plasmonic Crystals with Different Structure and Material Features. *Fabrication of Au Nanohole Arrays As Deposition Masks.* The Au nanohole arrays were made by a modified PEEL process.²⁸ Briefly, a poly(dimethylsiloxane) (PDMS) mask with square lattice spacing $a_0 = 600$ nm was used in phase-shifting photolithography to produce photoresist posts with diameter $d = 200$ nm on Si (100) wafers. After depositing a thin layer of Cr (10 nm) and lift-off PR posts, we used DRIE to create cylindrical pits beneath the circular Cr holes (diameter ~ 200 nm and depth ~ 150 nm) into the Si. Au nanohole arrays were then produced by depositing 100 nm Au and etching the Cr sacrificial layer.

Deposited Au Posts on Template-Stripped Au Film. Free-standing Au nanohole arrays were floated onto template-stripped Au films, and 35 nm Au was deposited by e-beam evaporation. The Au hole arrays were removed by scotch tape to result in deposited Au posts on an ultrasmooth Au film.

Deposited Ti Posts on Template-Stripped Au Film. Free-standing Au nanohole arrays were floated onto template-stripped Au films, and 35 nm Ti was deposited by e-beam evaporation. The Au hole arrays were removed by scotch tape to result in deposited Ti posts on an ultrasmooth Au film.

Template-Stripped Au Pyramid Arrays. Cr hole arrays on Si wafers were made by the PEEL process and functioned as KOH etching masks to produce pyramidal pits beneath the holes. Cr hole arrays were then removed and 100 nm Au was deposited by e-beam evaporation. The film was peeled with PU 61 to obtain stripped Au pyramid arrays.

Optical Measurements. *Normal Incidence Reflection Measurement.* An inverted microscope equipped with a spectrometer consisting of a 303 mm-focal-length monochromator and Andor Newton electron multiplication charge-coupled device (EM-CCD) camera was used for normal incidence reflection measurements. Incident light illumination was from a broadband halogen lamp. The reflected light from plasmonic crystals with an air superstrate was collected using a $1 \times$ Nikon microscope objective with a numerical aperture (NA) of 0.04. The reflected light from the plasmonic crystals in DMSO was collected using a $2 \times$ Nikon microscope objective with a NA = 0.06. The measured reflection from the plasmonic crystals were calibrated using the reflection spectra of the broadband dielectric mirror (Edmund Optics #64-114), which showed an average reflection of 99% between 350 and 1100 nm.

Angle-Resolved Reflectance Measurements. Plasmonic crystals were mounted on a computer-controlled stage that can rotate at incident angle (θ) with 0.02° accuracy. Collimated white light from a 100-W halogen source was incident on the plasmonic crystals, and the reflected light was directed to a CCD spectrometer (LN2-cooled CCD/Triax 522, Horiba Jobin Yvon). The reflectance spectra of the plasmonic crystals were measured under both p- (TM) and s- (TE) polarization from $\theta = 10\text{--}60^\circ$. The incident excitation plane was aligned along the high symmetry lattice direction.

Finite-Difference Time-Domain Simulations. Finite difference time domain (FDTD) calculations based on commercial software (FDTD Solutions, Lumerical, Inc., Vancouver, Canada) were used

to simulate reflectance from the plasmonic crystals. The optical constants of Au and Ti were taken from Johnson and Christy (550–950 nm)³² and Palik (550–950 nm),³³ respectively. A uniform mesh size of 2 nm (x, y, and z directions) was used. The size of the protruding Au or Ti posts was diameter $d = 200$ nm, spacing $a_0 = 600$ nm, and height $h = 20, 35$, and 50 nm. For deposited Au posts, we used a combination of 'rough_surface' and 'rough_wire' objects to produce Au posts with roughened surfaces. To calculate the angle and wavelength dependent reflectance spectra (dispersion diagram), we set perfectly matched layer (PML) boundary conditions for the z direction, and Bloch boundary conditions for x and y directions of the simulation region.

For the band structure calculations, a number of randomly orientated and randomly distributed dipole sources were used to ensure that all modes were excited. The fields over time were collected by randomly distributed time monitors and Fourier transformed to find the resonant frequencies. The band structure was then plotted after a parameter sweep over the Bloch vector k .

Lasing Measurements. A mode-locked Ti:sapphire laser with a regenerative amplifier (800 nm wavelength, 1-kHz repetition rate, 90 fs pulse width) was used to optically pump the device at an incident angle of 45°. The laser spot was about 0.2 cm². The emission was collected at different detection angles and then coupled into a bundled optical fiber connected to a compact spectrometer (USB 2000, Ocean Optics, 0.3 nm resolution). The laser beam was polarized along the high-symmetry axis of the square lattice. The spatial pattern and divergence angle of the lasing beam were analyzed using a high-resolution CCD beam profiler (LBR-HR, Newport, 1.4 Megapixel) placed normal to the sample surface.

Conflict of Interest: The authors declare no competing financial interest.

Acknowledgment. This work was supported by the National Science Foundation (NSF) under DMR-1306514 (W.W., T.W.O) and DMR-1121262 (A.Y., M.P.K., T.W.O., K.A.). Z.L. gratefully acknowledges support from the Ryan Fellowship and the Northwestern University International Institute for Nanotechnology. Research for this paper was conducted with Government support under FA9550-11-C-0028 (M.P.K and A.J.H) and awarded by Department of Defense, Air Force Office of Scientific Research, National Defense Science and Engineering Graduate (NDSEG) Fellowship, 32 CFR 168a. This work utilized Northwestern University Micro/Nano Fabrication Facility (NUFAB), which is supported by the State of Illinois and Northwestern University. This work made use of the EPIC facility (NUANCE Center-Northwestern University), which has received support from the MRSEC program (NSF DMR-1121262) at the Materials Research Center, and the Nanoscale Science and Engineering Center (EEC-0118025/003), both programs of the National Science Foundation; the State of Illinois; and Northwestern University. This research was supported in part through the computational resources and staff contributions provided for the Quest high performance computing facility at

Northwestern University, which is jointly supported by the Office of the Provost, the Office for Research, and Northwestern University Information Technology.

Supporting Information Available: The Supporting Information is available free of charge on the ACS Publications website at DOI: 10.1021/acsnano.5b05419.

Linear properties and lasing measurements of 2D plasmonic crystals with different structure and material features; SPP modes in Au plasmonic crystals; polarization of the output lasing beam for Ag plasmonic crystals (PDF)
Movie S1 (AVI)

REFERENCES AND NOTES

- Maier, S. A. *Plasmonics: Fundamentals and Applications*; Springer: New York, 2007.
- Ma, R.-M.; Yin, X.; Oulton, R. F.; Sorger, V. J.; Zhang, X. Multiplexed and Electrically Modulated Plasmon Laser Circuit. *Nano Lett.* **2012**, *12*, 5396–5402.
- Khurjin, J. B. How to Deal with the Loss in Plasmonics and Metamaterials. *Nat. Nanotechnol.* **2015**, *10*, 2–6.
- De Leon, I.; Berini, P. Amplification of Long-Range Surface Plasmons by a Dipolar Gain Medium. *Nat. Photonics* **2010**, *4*, 382–387.
- Zou, S.; Schatz, G. C. Narrow Plasmonic/Photonic Extinction and Scattering Line Shapes for One and Two Dimensional Silver Nanoparticle Arrays. *J. Chem. Phys.* **2004**, *121*, 12606–12612.
- Zheludev, N. I.; Prosvirnin, S. L.; Papasimakis, N.; Fedotov, V. A. Lasing Spaser. *Nat. Photonics* **2008**, *2*, 351–354.
- Li, Z.; Butun, S.; Aydin, K. Ultranarrow Band Absorbers Based on Surface Lattice Resonances in Nanostructured Metal Surfaces. *ACS Nano* **2014**, *8*, 8242–8248.
- Yang, A.; Hoang, T. B.; Dridi, M.; Deeb, C.; Mikkelsen, M. H.; Schatz, G. C.; Odom, T. W. Real-Time Tunable Lasing From Plasmonic Nanocavity Arrays. *Nat. Commun.* **2015**, *6*, 6939.
- Kravets, V.; Schedin, F.; Grigorenko, A. Extremely Narrow Plasmon Resonances Based on Diffraction Coupling of Localized Plasmons in Arrays of Metallic Nanoparticles. *Phys. Rev. Lett.* **2008**, *101*, 087403.
- Augué, B.; Barnes, W. Collective Resonances in Gold Nanoparticle Arrays. *Phys. Rev. Lett.* **2008**, *101*, 143902.
- Vecchi, G.; Giannini, V.; Gómez Rivas, J. Surface Modes in Plasmonic Crystals Induced by Diffractive Coupling of Nanoantennas. *Phys. Rev. B: Condens. Matter Mater. Phys.* **2009**, *80*, 201401.
- Bergman, D.; Stockman, M. Surface Plasmon Amplification by Stimulated Emission of Radiation: Quantum Generation of Coherent Surface Plasmons in Nanosystems. *Phys. Rev. Lett.* **2003**, *90*, 027402.
- Stockman, M. I. The Spaser as a Nanoscale Quantum Generator and Ultrafast Amplifier. *J. Opt.* **2010**, *12*, 024004.
- Oulton, R. F.; Sorger, V. J.; Zentgraf, T.; Ren-Min, M.; Gladden, C.; Dai, L.; Bartal, G.; Zhang, X. Plasmon Lasers at Deep Subwavelength Scale. *Nature* **2009**, *461*, 629–632.
- Noginov, M. A.; Zhu, G.; Belgrave, A. M.; Bakker, R.; Shalaev, V. M.; Narimanov, E. E.; Stout, S.; Herz, E.; Suteewong, T.; Wiesner, U. Demonstration of a Spaser-Based Nanolaser. *Nature* **2009**, *460*, 1110–1112.
- Zhou, W.; Dridi, M.; Suh, J. Y.; Kim, C. H.; Co, D. T.; Wasielewski, M. R.; Schatz, G. C.; Odom, T. W. Lasing Action in Strongly Coupled Plasmonic Nanocavity Arrays. *Nat. Nanotechnol.* **2013**, *8*, 506–511.
- Lu, Y. J.; Kim, J.; Chen, H. Y.; Wu, C.; Dabidian, N.; Sanders, C. E.; Wang, C. Y.; Lu, M. Y.; Li, B. H.; Qiu, X.; et al. Plasmonic Nanolaser Using Epitaxially Grown Silver Film. *Science* **2012**, *337*, 450–453.
- Yang, A.; Odom, T. Advances in Plasmonic Nanolasers. *IEEE Photonics J.* **2015**, *7*, 0700606.
- Lu, Y.-J.; Wang, C.-Y.; Kim, J.; Chen, H.-Y.; Lu, M.-Y.; Chen, Y.-C.; Chang, W.-H.; Chen, L.-J.; Stockman, M. I.; Shih, C.-K.; et al. All-Color Plasmonic Nanolasers with Ultralow Thresholds: Autotuning Mechanism for Single-Mode Lasing. *Nano Lett.* **2014**, *14*, 4381–4388.
- van Beijnum, F.; van Veldhoven, P. J.; Geluk, E. J.; de Dood, M. J. A.; Hooft, G. W. T.; van Exter, M. P. Surface Plasmon Lasing Observed in Metal Hole Arrays. *Phys. Rev. Lett.* **2013**, *110*, 206802.
- Meng, X.; Liu, J.; Kildishev, A. V.; Shalaev, V. M. Highly Directional Spaser Array for the Red Wavelength Region. *Laser & Photon. Rev.* **2014**, *8*, 896–903.
- Schokker, A. H.; Koenderink, A. F. Lasing at the Band Edges of Plasmonic Lattices. *Phys. Rev. B: Condens. Matter Mater. Phys.* **2014**, *90*, 155452.
- Rogers, J. A.; Paul, K. E.; Jackman, R. J.; Whitesides, G. M. Using an Elastomeric Phase Mask for Sub-100 nm Photolithography in the Optical Near Field. *Appl. Phys. Lett.* **1997**, *70*, 2658.
- Reichel, F.; Jeurgens, L. P. H.; Richter, G.; Mittemeijer, J. Amorphous versus Crystalline State for Ultrathin Al₂O₃ Overgrowths on Al Substrates. *J. Appl. Phys.* **2008**, *103*, 093515.
- Henry, M. D.; Walavalkar, S.; Homyk, A.; Scherer, A. Alumina Etch Masks for Fabrication of High-Aspect-Ratio Silicon Micropillars and Nanopillars. *Nanotechnology* **2009**, *20*, 255305.
- Genet, C.; Ebbesen, T. W. Light in Tiny Holes. *Nature* **2007**, *445*, 39–46.
- Degiron, A.; Lezec, H. J.; Barnes, W. L.; Ebbesen, T. W. Effects of Hole Depth on Enhanced Light Transmission Through Subwavelength Hole Arrays. *Appl. Phys. Lett.* **2002**, *81*, 4327–4329.
- Henzie, J.; Lee, M. H.; Odom, T. W. Multiscale Patterning of Plasmonic Metamaterials. *Nat. Nanotechnol.* **2007**, *2*, 549–554.
- Amnon, Y. *Optical Electronics in Modern Communications*, 5 ed.; Oxford University Press: New York, 1997.
- Czikkely, V.; Forsterling, H. D.; Kuhn, H. Extended Dipole Model for Aggregates of Dye Molecules. *Chem. Phys. Lett.* **1970**, *6*, 207–210.
- Suh, J. Y.; Kim, C. H.; Zhou, W.; Huntington, M. D.; Co, D. T.; Wasielewski, M. R.; Odom, T. W. Plasmonic Bowtie Nanolaser Arrays. *Nano Lett.* **2012**, *12*, 5769–5774.
- Johnson, P. B.; Christy, R. W. Optical Constants of the Noble Metals. *Phys. Rev. B* **1972**, *6*, 4370.
- Palik, E. D. *Handbook of Optical Constants of Solids*; Academic: Orlando, FL, 1985.